

Structural and magnetic properties of a new cubic spinel LiRhMnO₄

S. Kundu,^{1,*} T. Dey,² M. Prinz-Zwick,³ N. Büttgen,³ and A. V. Mahajan^{1,†}

¹*Department of Physics, Indian Institute of Technology Bombay, Powai, Mumbai 400076, India*

²*Experimental Physics VI, Center for Electronic Correlations and Magnetism,
University of Augsburg, 86159 Augsburg, Germany*

³*Experimental Physics V, Center for Electronic Correlations and Magnetism,
University of Augsburg, 86159 Augsburg, Germany*

(Dated: December 15, 2024)

Abstract

We report the structural and magnetic properties of a new system LiRhMnO₄ (LRMO) through x-ray diffraction, bulk magnetization, heat capacity and ⁷Li nuclear magnetic resonance (NMR) measurements. LRMO crystallizes in the cubic space group $Fd\bar{3}m$. From the DC susceptibility data, we obtained the Curie-Weiss temperature $\theta_{CW} = -26$ K and Curie constant $C = 1.79$ Kcm³/mol suggesting antiferromagnetic correlations among the magnetic Mn⁴⁺ ions with an effective spin $S = \frac{3}{2}$. At $H = 50$ Oe, the field cooled and zero-field cooled magnetizations bifurcate at a freezing temperature, $T_f = 4.45$ K, which yields the frustration parameter $f = \frac{|\theta_{CW}|}{T_f} > 5$. AC susceptibility, shows a cusp-like peak at around T_f , with the peak position shifting as a function of the driving frequency, confirming a spin-glass-like transition in LRMO. LRMO also shows typical spin-glass characteristics such as memory effect, aging effect and relaxation. In the heat capacity, there is no sharp anomaly down to 2 K indicative of long-range ordering. The field sweep ⁷Li NMR spectra show broadening with decreasing temperature without any spectral line shift. The ⁷Li NMR spin-lattice and spin-spin relaxation rates also show anomalies due to spin freezing near T_f .

PACS numbers: 75.50.Lk, 75.40.Cx, 76.60.-k

I. INTRODUCTION

In the last few decades, most of the scientific work in condensed matter physics has chiefly been devoted to study the strongly correlated electron systems (SCES) [1, 2]. Materials with strong electronic correlations are the materials, in which the movement of one electron depends on the positions and movements of all other electrons due to the long-range Coulomb interaction (U). In this regard, the transition metal oxide (TMO) compounds [3] have become the centre stage of attraction to physicists, since the TMO have outermost electrons in d-orbitals which are strongly localized. Hence, the electron density is no longer homogeneous and the striking properties of the system are in fact dependent on the presence of strong electron-electron interactions. Also, the frustration in TMO, either imposed by the geometry of the spin system or by the competing interactions, leads to exotic behavior [4–7]. The rich physics of magnetically frustrated systems, continues to attract interest in the condensed matter research community. The resurgence of interest began with the discovery of high- T_c superconductivity (observed in layered cuprates [8] in the late 80's and pnictides [9] more recently), and novel phenomenon such as metal-insulator transition (MIT) [10], colossal magneto-resistance (CMR) [11], charge ordering and quantum magnetism. It was soon realized that the strong interplay of spin, charge, lattice and orbital degrees of freedom in these correlated systems resulted in

such diverse properties. In recent years, the interest in solids containing lithium ions has increased profoundly due to the potential applications in long-lasting rechargeable batteries. In this regard, the spinel oxide LiMn₂O₄ has attracted wide attention as a cathode material of batteries due to its low cost and non-toxicity [12, 13]. At room temperature LiMn₂O₄ [14] crystallizes in the cubic space group $Fd\bar{3}m$, with the following cation distribution $(\text{Li}^+)_{\text{A}}[\text{Mn}^{3+}\text{Mn}^{4+}]_{\text{B}}\text{O}_4$; here the subscripts A and B denote the tetrahedral and octahedral sites, respectively. Likewise, Takagi *et al.* found the metal-insulator transition (MIT) property in LiRh₂O₄ [15–17], which behaves like a paramagnetic metal at high temperature; whereas below about 170 K it becomes a valence bond insulator and the ground state of mixed-valent $\text{Li}[\text{Rh}^{3+}(S=0)\text{Rh}^{4+}(S=\frac{1}{2})]\text{O}_4$ is charge frustrated. How will the ground state of this system vary if one replaces the $S = \frac{1}{2}$ ion with higher spin ions, say $S = \frac{3}{2}$? With this motivation, we decided to explore LiRhMnO₄ (LRMO) which is structurally identical to LiMn₂O₄ but magnetically different. Magnetic properties of LRMO have so far not been reported. Only the structure of LRMO was first reported long back in 1963 by G. Blasse [18]. It is a mixed metal oxide with spinel structure [19] where 50% of the B-sites are occupied by non-magnetic Rh³⁺ ($S = 0$) and the other 50% by magnetic Mn⁴⁺ ($S = \frac{3}{2}$) ions. Usually, the B-site spinel has a corner-shared tetrahedral network like the pyrochlore lattice which is geometrically frustrated. But due to the B-site disorder, the frustration may be relieved and result in a spin-glass state [20] at a low T .

We have synthesized polycrystalline LRMO and studied its bulk and local magnetic properties through various characterization techniques such as x-ray diffraction,

*Electronic address: skundu37@gmail.com

†Electronic address: mahajan@phy.iitb.ac.in

DC and AC magnetization, heat capacity and field sweep ^7Li nuclear magnetic resonance (NMR). We found that LRMO has antiferromagnetic (AFM) correlations among Mn^{4+} ions and conventional spin-glass ground state with the spin-freezing temperature $T_f = 4.45$ K.

II. EXPERIMENTAL DETAILS

Polycrystalline LRMO was prepared by solid-state reaction. Pre-heated starting materials (Li_2CO_3 , Rh metal powder and MnO_2) were mixed in stoichiometry and ground thoroughly for hours. Finally a hard pellet was made and calcined at 500°C , 700°C , 900°C and 1050°C for 24 hours each time. As there is a chance of lithium evaporation above 900°C , 15% excess Li_2CO_3 was mixed to get the pure LRMO. The processes of grinding and firing were done until we obtained the single phase sample. The single phase of LRMO is confirmed from the powder x-ray diffraction (XRD) measurements at room temperature with $\text{Cu } K_\alpha$ radiation ($\lambda = 1.54182 \text{ \AA}$) on a PANalytical X'Pert PRO diffractometer. DC and AC magnetization data were measured as a function of temperature T (2 K – 400 K) with the applied field H (0 – 70 kOe) and the frequency ν (1 Hz–1000 Hz) using a commercial superconducting quantum interference device (SQUID) magnetometer. Low-field magnetization measurements were performed utilizing the reset magnet mode option of the SQUID. Heat capacity measurements were performed in the temperature T (2 K – 215 K) and in the field H (0 – 90 kOe) using the heat capacity option of a Quantum Design PPMS. As the ^7Li NMR spectra are very broad especially at low- T and it is difficult to obtain the full line-shape only by the Fourier transform of the time echo signal in our fixed field NMR setup, we have performed field sweep ^7Li NMR measurements at 60 MHz and 95 MHz. The spin-lattice relaxation rate ($\frac{1}{T_1}$) is measured by the saturation recovery method and the spin-spin relaxation rate ($\frac{1}{T_2}$) is obtained by measuring the decay of the echo integral with variable delay time.

Table I: Atomic coordinates of LRMO

Atom	Wyckoff position	x	y	z	Occupancy
Li	8a	0.125	0.125	0.125	1.00
Rh	16d	0.500	0.500	0.500	0.50
Mn	16d	0.500	0.500	0.500	0.50
O	32e	0.747	0.747	0.747	1.00

III. RESULTS AND DISCUSSION

A. Crystal structure

The powder XRD data has been recorded with $\text{Cu-}K_\alpha$ radiation over the angular range $15^\circ \leq 2\theta \leq 98^\circ$ in

0.004° step size and treated by profile analysis using the Rietveld refinement [21] by Fullprof suite [22] program. From the XRD pattern analysis, we found that the prepared LRMO is crystallized in single phase and there is no sign of any unreacted ingredients or impurity phases. The Rietveld refinement of XRD pattern is shown in Fig. 1. From refinement, we obtained the cell parameters of LRMO, $a = b = c = 8.319 \text{ \AA}$ (which is close to the earlier reported value 8.30 \AA [18]), $\alpha = \beta = \gamma = 90^\circ$ and the atomic coordinates of LRMO is given in Table I. The reliability of the x-ray refinement of LRMO is given by the following parameters χ^2 : 4.63; R_p : 2.98%; R_{wp} : 5.68%; R_{exp} : 2.63%.

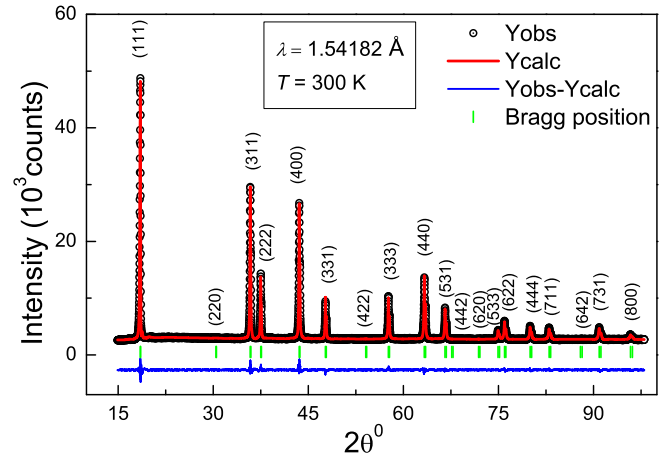


Figure 1: The Rietveld refinement of room temperature powder XRD pattern of LRMO is shown along with its Bragg peak positions (green vertical marks) and the corresponding Miller indices (hkl).

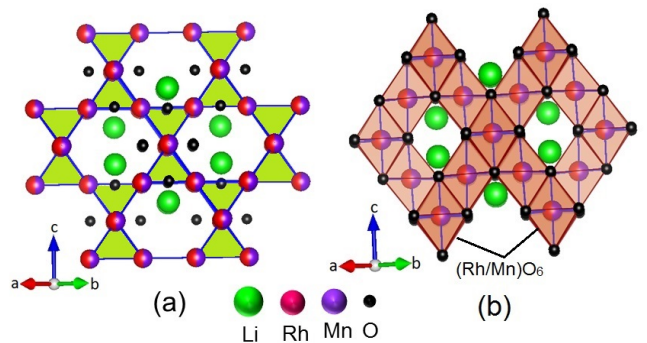


Figure 2: Structure of LRMO (a) The corner shared tetrahedral network of (Rh/Mn) atoms in 3-dimension. (b) one unit cell is shown with the edge-shared (Rh/Mn) O_6 octahedra.

The structure of LRMO has been drawn and analyzed by using Vesta software [23]. We have obtained the atomic coordinates from Rietveld refinement done on XRD pattern of LRMO which crystallizes in the non-centrosymmetric cubic spinel structure $Fd\bar{3}m$ (space

group 227). The Rh or Mn atoms are connected to each other via a tetrahedral network as shown in Fig. 2(a). These tetrahedra are corner-shared and form a geometrically frustrated magnetic system. In the structure, (Rh/Mn)O₆ form perfect octahedra with (Rh/Mn)-O bond distance 2.055 Å (shown in Fig. 2(b)). The presence of non-magnetic Rh³⁺ ($S = 0$) at the B-site of the spinel, *i.e.* in a tetrahedral unit, distorts the corner-shared arrangement of Mn⁴⁺ ($S = \frac{3}{2}$) ions. This makes the B-sites diluted.

B. Bulk magnetization

1. DC susceptibility

The temperature dependence of the bulk dc magnetic susceptibility $\chi(T) = \frac{M(T)}{H}$ is measured on LRMO under different applied magnetic fields in the temperature range of (2-400) K. The main features of our observations from the dc susceptibility measurement are discussed here. With increasing fields, the $\chi(T)$ reduces in the low temperature region (see inset of Fig. 3). Below 5 K, there is splitting between the zero-field cooled (ZFC) and field cooled (FC) data at $H = 50$ Oe and 500 Oe as shown in the inset of Fig. 3. Also, the $\chi(T)$ below 500 Oe shows some anomaly around 5 K. This may be due to regular antiferromagnetic (AFM) ordering which is very sensitive to the applied field as splitting between ZFC-FC is suppressed with fields higher than 5 kOe. The existence of ZFC-FC splitting below 500 Oe suggests the presence of a glassy state below 5 K. This is a signature of conventional spin-glass [24]. Fig. 3 shows the paramagnetic behavior of the dc susceptibility at 20 kOe. The Curie-Weiss fitting in the high temperature region (200-400 K) gives a Curie constant $C = 1.79$ Kcm³/mol and a Curie-Weiss temperature $\theta_{CW} = -26$ K. The negative value of the Curie-Weiss temperature suggests AFM interaction among the magnetic Mn⁴⁺ ions. The effective moment of Mn⁴⁺ ions [using $C = 1.79$ Kcm³/mol] is $\mu_{\text{eff}} = 3.78 \mu_B$ which is close to the expected value $3.87 \mu_B$ for the Mn⁴⁺ ion.

2. AC susceptibility

The ac susceptibility is measured by keeping the dc applied field to be zero and with an ac field H_{ac} of 3.5 Oe amplitude. The frequency dependence of the in-phase component $\chi'_{ac}(T)$ is shown in Fig. 4. The freezing temperature (T_f) shifts towards higher temperatures as the frequency increases which are typical features in glassy systems [25]. Also, the out of phase component of the ac susceptibility $\chi''_{ac}(T)$ has a frequency dependence with an anomaly around T_f . The $\chi'_{ac}(T)$ is non-zero positive below T_f and is negative above T_f . All these above features point to the formation of a spin-glass ground state. The frequency dependence of T_f is often quantified in terms of the relative shift of the spin-freezing temperature, defined as $\delta T_f = [\Delta T_f / T_f \Delta \log_{10}(\nu)]$ [26], which is calculated to be 0.022 for the LRMO compound. This

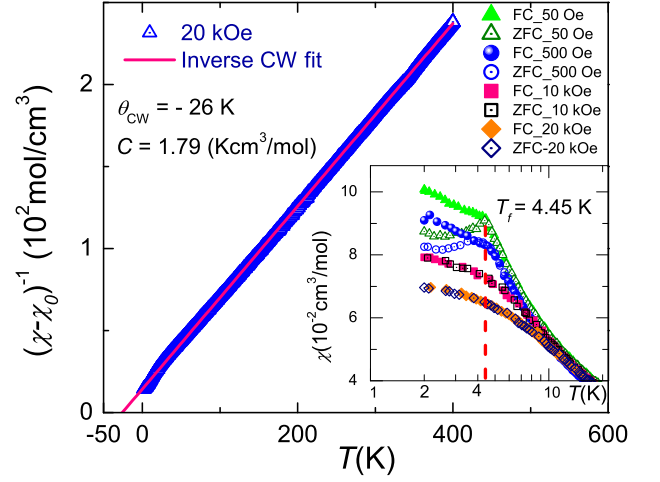


Figure 3: The temperature dependence of $\chi(T)$ of LRMO at $H = 20$ kOe. The inset, (semi-log scale) shows the ZFC-FC bifurcation below 4.45 K at different applied fields.

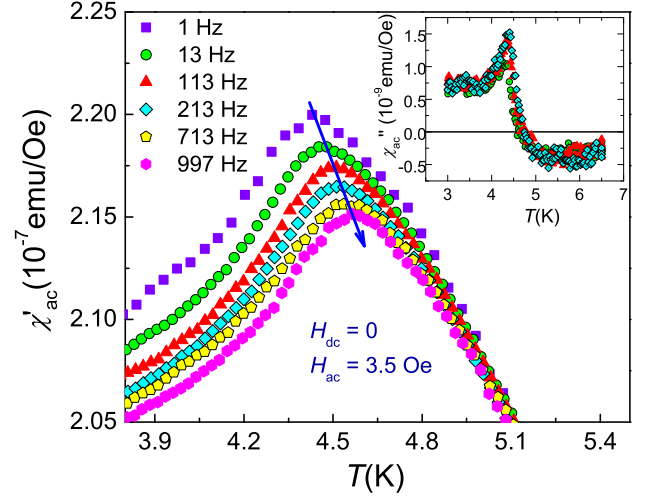


Figure 4: The in-phase component of ac susceptibility $\chi'_{ac}(T)$ of LRMO as a function of temperature at different frequencies are shown in the main figure. In the inset, the out of phase component of ac susceptibility is shown.

value of δT_f which determines the sensitivity to the frequency falls in between the value of canonical spin-glass systems and superparamagnets. It is of interest to note that the present value is close to 0.037 which is observed for metallic glasses [27].

The Vogel-Fulcher fit by equation ($\omega = \omega_0 \exp[-E_a/k_B(T_f - T_0)]$) of the variations of the freezing temperature (T_f) with frequency suggests short-range Ising spin-glass behavior [28] (shown in Fig. 5). From the fit, we obtained the activation energy $E_a/k_B \approx 3.46$ K, the characteristic angular frequency $\omega_0 \approx 1.01 \times 10^8$ rad/s and the Vogel-Fulcher temperature $T_0 \approx 4.22$ K. For a conventional spin-glass system, ω_0 is of the order of 10^{13} rad/s. So the obtained ω_0 value is small compared to that of a usual spin-glass system.

This large deviation may not be the true scenario as the error involved in determining the freezing temperature is large and the measured frequency range is limited to only two decades.

The variation of the freezing temperature T_f with frequency obey with the critical slowing down dynamics (see Fig. 5) which is expressed by the equation: $\tau = \tau_0 (T_f / T_g - 1)^{-zv}$. Here τ_0 is the relaxation time and zv is the dynamic exponent [29]. We found the best fit with $T_g = 4.38$ K, $\tau_0 \approx 2.85 \times 10^{-10}$ s and $zv \approx 4.88$. The value of τ_0 is 10^{-10} to 10^{-13} s and zv lies in between of 4 - 13 for the conventional spin-glass systems [27]. The present values of τ_0 and zv imply that the ground state of LRMO is a conventional spin-glass.

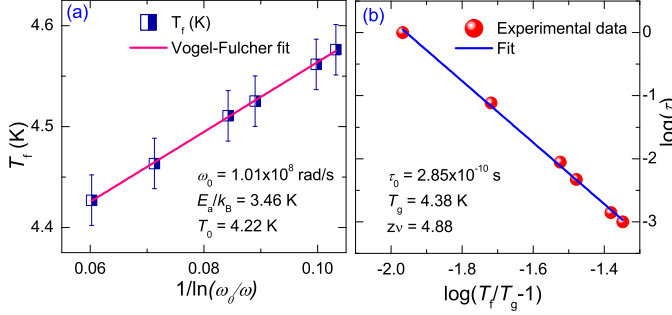


Figure 5: (a) The Vogel-Fulcher fit of the freezing temperatures T_f at different frequencies of the LRMO sample. (b) A fit of the T_f by the critical slowing down equation.

3. Memory effect

Fig. 6 shows a memory effect in LRMO. We have measured the field cooled (FC) magnetization using the protocol described by Sun *et al.*[30, 31]. We have recorded the magnetization by cooling the LRMO sample down to 1.85 K with a cooling rate of 1 K/min and an applied field of 300 Oe. We have interrupted the cooling process below T_f i.e. at 2.8 K and 2.3 K for a waiting time (t_w) of 2 hours. We switched off the field during t_w , allowed the system to relax and resumed the measurement after each stop and wait period. Fig. 6 shows step-like features which are the evidence of stops at 2.8 K and 2.3 K in the FC stop curve. Then we have recorded the magnetization of the sample while heating continuously at the same field of 300 Oe. We also have measured a reference curve named as “FC cooling” by simply cooling the sample continuously at $H = 300$ Oe. We have noticed a change of slope at 2.8 K and a prominent minimum at 2.3 K in the FC warming curve. So the system can remember its previous behavior during the cooling operation imprinted as a memory. This sort of behavior has been observed in inter-metallic compounds such as GdCu [32], Nd₅Ge₃[33]) and in super spin glass nanoparticle systems [30, 34]. This is one of the typical characteristics of spin-glasses.

To know further features of the memory effect, we have measured the magnetic relaxation in ZFC and FC

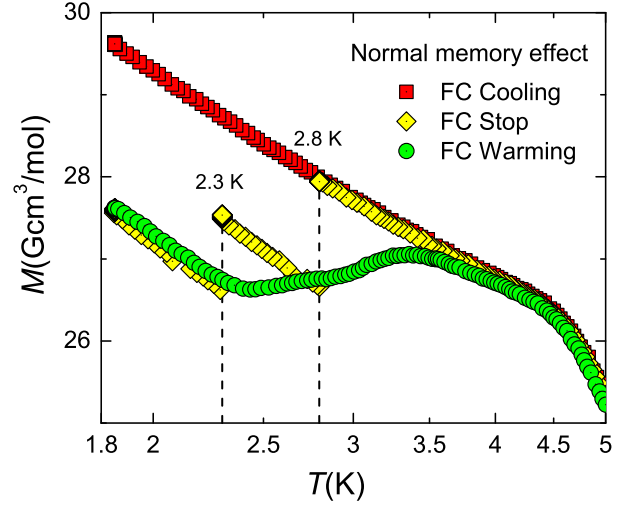


Figure 6: The memory effect in the field cooled (FC) magnetization data of LRMO is plotted. The FC stop curve is measured during the cooling of the LRMO sample in a field of 300 Oe with a relaxation at 2.8 K and 2.3 K for two hours, whereas the FC warming curve is measured with continuous heating and the reference curve, FC cooling, is measured by continuously cooling LRMO at $H = 300$ Oe without any break.

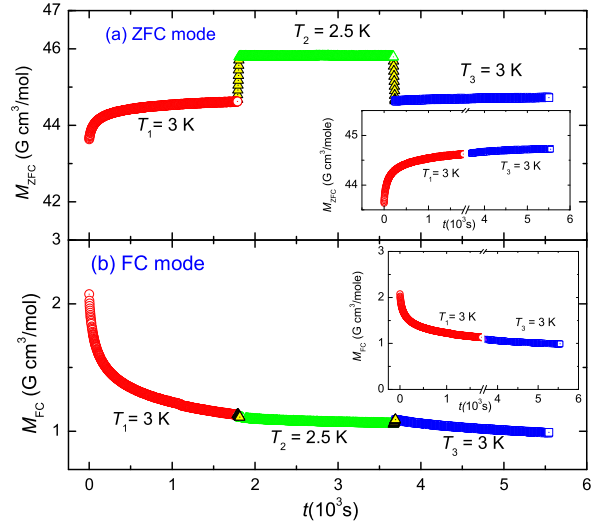


Figure 7: Magnetic relaxation in LRMO at 3 K with a temporary quench to 2.5 K in (a) the ZFC mode and (b) the FC mode. Insets show continuity in the relaxation data during temperature T_1 and T_3 in both mode.

mode with a negative and a positive temperature cycling as shown in Fig. 7 and Fig. 8 respectively. We have recorded each relaxation curve for $\frac{1}{2}$ hour. In the ZFC mode, we have cooled the sample in the absence of field but measured the data with an applied field of $H = 500$ Oe. In contrast to that, in the FC mode, the field ($H = 500$ Oe) is continuously on during cooling of the sample and switched off just before the measurement starts.

In the negative heat cycle, we have quenched the system to a lower temperature and resumed the relaxation process. The initial and final relaxation data are at $T_1 = T_3 = 3\text{ K}$ whereas the quenched one is at $T_2 = 2.5\text{ K}$. Fig. 7 (a) and (b) shows the relaxation data in ZFC and FC mode in the negative heat cycle process. If we ignore the middle one, the initial and the final relaxation are just a continuation of each other as shown in the inset of Fig. 7 (a) and (b). So in the negative heat cycle or the temporary quenching, the system remembers the earlier states where it was, irrespective of the measurement processes i.e. either ZFC or FC mode. This is the memory effect in negative heating cycle.

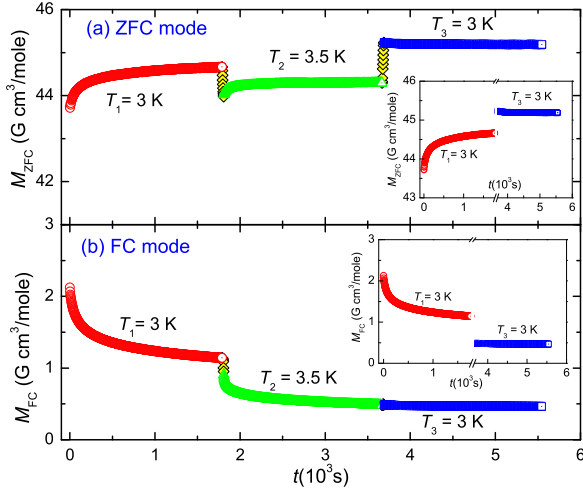


Figure 8: The magnetic relaxation in LRMO with a positive heating cycle in (a) ZFC mode and (b) FC mode. Insets show discontinuity in the relaxation data at T_1 and T_3 in both mode.

We also have measured magnetization in a temporary heating cycle in order to compare the response with the cooling cycles. In the positive heat cycle, we have increased the temperature of the middle step to $T_2 = 3.5\text{ K}$ whereas the initial and final steps are at $T_1 = T_3 = 3\text{ K}$. Fig. 8 (a) and (b) show the relaxation data in ZFC and FC mode respectively. From the inset of Fig. 8, it is very clear that the relaxations at T_1 and T_3 are discontinuous and the response of the system is asymmetric. So the positive heat cycle erases the memory in both ZFC and FC processes. This supports the hierarchical model as proposed for the spin-glasses.

4. Ageing effect and relaxation

The Fig. 9 shows the ageing effect in the dc magnetization data. Below the freezing temperature, that is at 2.5 K , the growth of the magnetization is recorded as a function of time in the ZFC mode with an applied field of $H = 200\text{ Oe}$ after a different waiting time (t). We have waited for three different times like 10 s , 1000 s and 5000 s . From our plot, it is obvious that the magnetization growth is faster for small waiting

time and slower for large waiting time. These point towards the formation of metastable state associated with the low temperature magnetic state. We also mea-

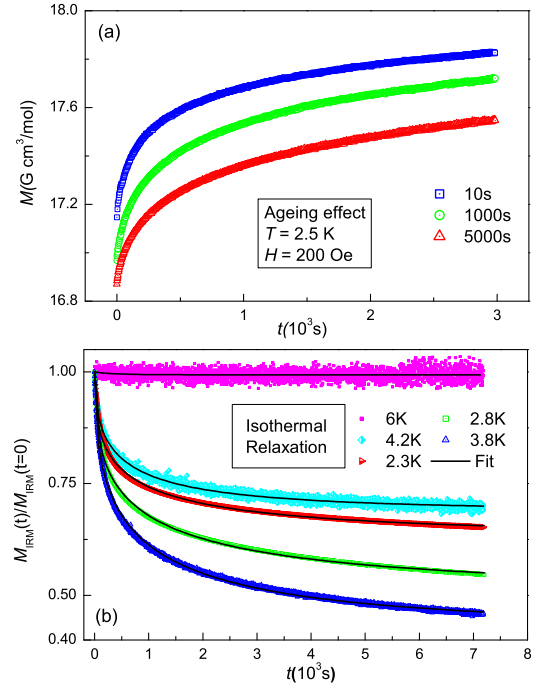


Figure 9: (a) Ageing effect of the dc magnetization of LRMO as a function of time with intervals of 10 s , 1000 s and 5000 s . (b) The normalized isothermal remanent magnetization is shown as a function of time. The data are well fitted with a stretched exponential as described in text.

sured the isothermal remanent magnetization (M_{IRM}) of LRMO to explore the metastable behavior of the glassy state below the spin-glass transition temperature. For this, a field of 300 Oe was applied for 300 s after we cooled the LRMO sample in the zero field mode and reached a particular temperature and then the applied field was switched off and let the system to relax for 2 hours at that temperature. During relaxation, the magnetization data was then recorded as a function of time. Fig. 9 shows the decay curves normalized to the magnetization before making the field zero, $M_{\text{IRM}}(t)/M_{\text{IRM}}(0)$. These isothermal remanent magnetization were well fitted with stretched exponential ($M_t(H) = M_0(H) + [M_\infty(H) - M_0(H)][1 - \exp\{-t/\tau\}^\alpha]$) and from the fitting, we obtained the characteristic relaxation time (τ) at different temperatures (shown in Fig. 9). Here α is the stretching exponent ($0 \leq \alpha \leq 1$), M_0 and M_∞ are the magnetization at when $t \rightarrow 0$ and $t \rightarrow \infty$ respectively. The best fit parameters obtained for each isotherm is listed in Table II. It is natural that the decay of M_{IRM} is faster for temperature closer to T_f . This signifies that the system forms a metastable and irreversible state below T_f . As expected, above T_f i.e. at 6 K , M_{IRM} is independent of time.

Table II: The best fit result of each isothermal relaxation of LRMO fitted by stretched exponential.

$T(K)$	$\frac{M_\infty}{M_0}$	Stretching exponent α	Relaxation time $\tau(s)$
3.8	0.43	0.45	770
2.8	0.51	0.42	877
2.3	0.63	0.42	638
4.2	0.69	0.47	526

C. Heat capacity

The heat capacity $C_p(T)$ of magnetic LRMO was measured at different fields (0 - 90 kOe) in the temperature range 1.8- 300 K. There is no sharp anomaly in the $C_p(T)$ vs. T data as might usually be expected at an LRO transition. In the inset of Fig. 10, $C_p(T)/T$ vs. T , there is no significant influence of the applied magnetic field on the heat capacity. Also, no Schottky type anomaly was found in this system at the low temperature.

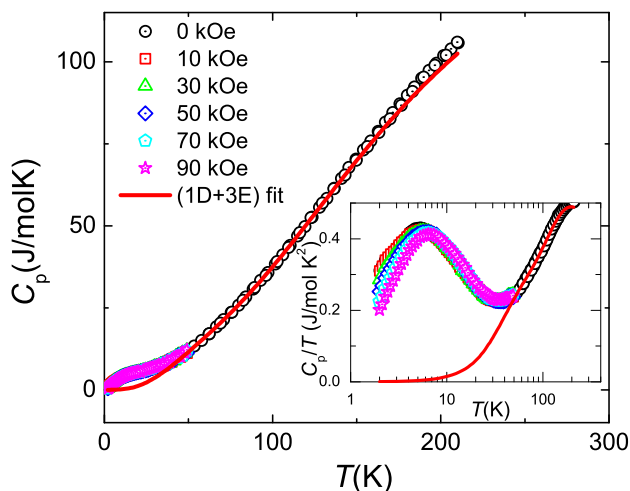


Figure 10: Main figure shows the total heat Capacity $C_p(T)$ of LRMO measured at different fields with Debye-Einstein fit (see text). In the inset $C_p(T)/T$ vs. T plot shows the prominent magnetic contribution to the C_p .

The total heat capacity of LRMO has the contribution from lattice (C_{lat}) and magnetic (C_m) both. As there was no suitable non-magnetic analogue available we have fitted the data with Debye term $\left(C_d \left[9nR \left(\frac{T}{\theta_D}\right)^3 \int_0^{x_D} \frac{x^4 e^x}{(e^x - 1)^2} dx\right]\right)$ and several Einstein terms $\left(\sum C_{e_i} \left[3nR \left(\frac{\theta_{E_i}}{T}\right)^2 \frac{\exp\left(\frac{\theta_{E_i}}{T}\right)}{\left(\exp\left(\frac{\theta_{E_i}}{T}\right) - 1\right)^2}\right]\right)$ in the T -range (55-130) K and then extrapolated to low- T to determine the C_{lat} . Among them, one Debye function plus two Einstein functions (1D+2E) fit was the best where the coefficients C_d and C_{e_i} accounts for the relative weight of the acoustic and optical modes of vibrations respectively. After fitting we obtained $C_d:C_{e_1}:C_{e_2} = 1:1:5$. The sum of these coefficients is equal to the to-

tal number of atoms ($n = 7$) per formula unit of LRMO. The deviation of the $C_p(T)$ from the Debye-Einstein fit below 50 K indicates the presence of a significant magnetic contribution to the heat capacity. The magnetic heat capacity $C_m(T)$ is obtained by subtracting the lattice contribution from total heat capacity and shown in Fig. 11 on the left y -axis. The magnetic heat capacity is almost independent of the strength of the applied field. It shows a hump around 18 K which indicates onsets of short-range interactions among the magnetic atoms. Also the magnetic entropy change $\Delta S_m(T)$ is calculated using $\Delta S_m = \int \frac{C_m}{T} dT$ relation and shown in the right y -axis of Fig. 11. Its value is 8.55 (J/mol K) which is 75% of the expected 11.52 (J/mol K) for $S = \frac{3}{2}$ spin. Considering the uncertainty involved in determining the lattice specific heat, the value of ΔS_m obtained is not far from the expected value.

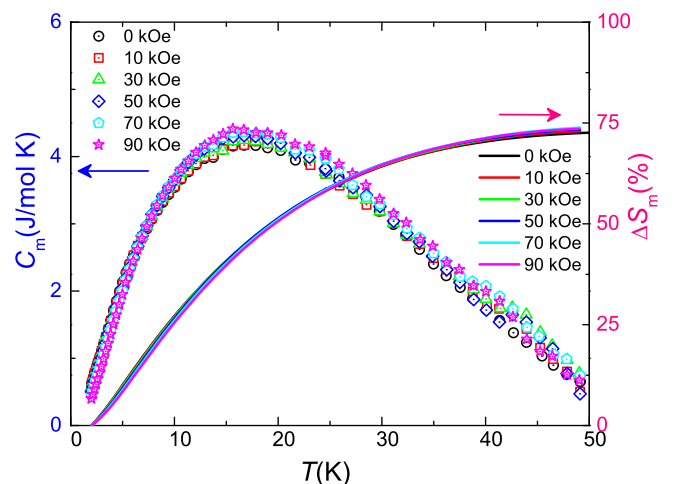


Figure 11: The magnetic heat capacity $C_m(T)$ on left y -axis and the magnetic entropy change $\Delta S_m(T)$ on the right y -axis of LRMO sample are shown.

D. ${}^7\text{Li}$ NMR Result

${}^7\text{Li}$ nuclei has a high natural abundance (92.6%) and it has nuclear spin $I = \frac{3}{2}$ with the value of gyromagnetic ratio $\frac{\gamma}{2\pi} = 16.54607$ (MHz/T). We have measured the field sweep ${}^7\text{Li}$ NMR at 60 MHz and 95 MHz. We also measured spin-lattice relaxation rate ($1/T_1$) and the spin-spin relaxation rate ($1/T_2$) at 60 MHz ($H \sim 36$ kOe). These measurements throw light on the nature of the intrinsic interactions of magnetic atoms.

1. ${}^7\text{Li}$ NMR Spectra

For the spectra, we use the optimal pulse sequence $(\pi/2 - \tau - \pi) = 5 \mu\text{s} - 100 \mu\text{s} - 10 \mu\text{s}$ at 60 MHz. The 100 μs refers to the time duration between the starting of the two pulses. The spectra at different temperatures (from

92.7 K to 2.6 K) are shown in Fig. 12. There is no significant shift in the spectra. The lithium surroundings in one unit cell are shown in the inset of Fig. 12. From the spectra, we have obtained the full width at half maxima (FWHM) at different temperatures which track the dc susceptibility well as shown in Fig. 13.

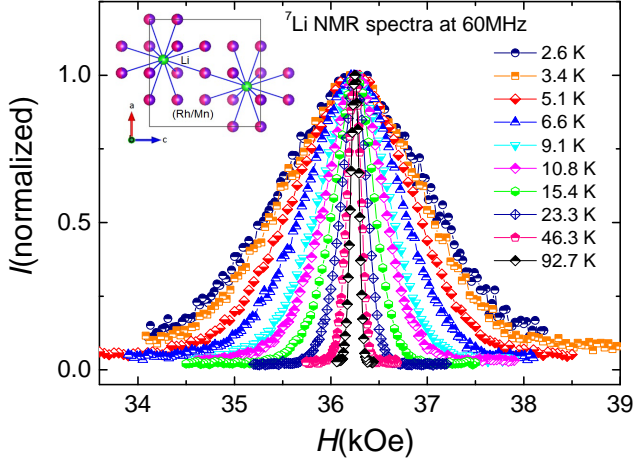


Figure 12: Normalized ${}^7\text{Li}$ NMR spectra of LRMO measured at 60 MHz frequency and at different temperatures down to 2.6 K.

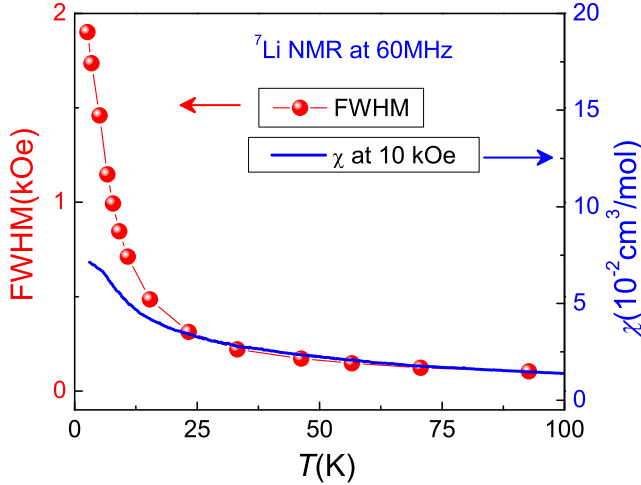


Figure 13: The FWHM (shown on left y -axis) follows the bulk dc susceptibility (on right y -axis) at high- T .

The ${}^7\text{Li}$ spectra at different temperatures are plotted without normalization of the spin-echo intensity I as a function of sweep field H (see Fig. 14). On lowering the temperature the total spectral intensity is constant down to about 20 K and then begins to decrease below 20 K. In the inset of Fig. 14, the echo integral (which is obtained by integrating the line-shape as a function of field *i.e.* the area under the spectrum at a particular temperature) times the temperature is plotted as a function of temperature. It shows a drop below 20 K. This suggests a

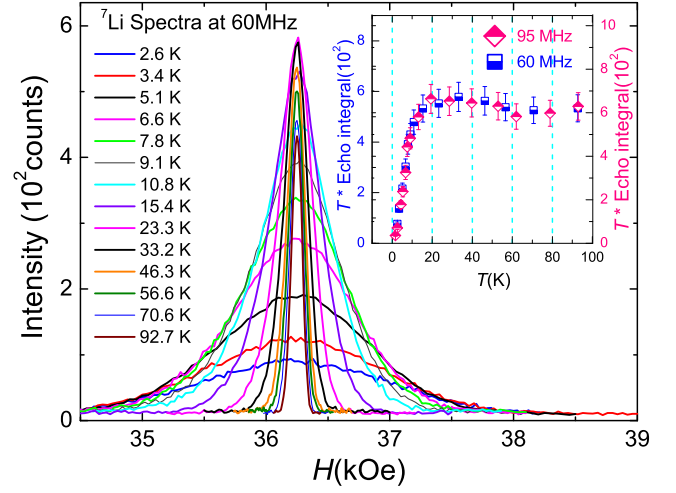


Figure 14: The ${}^7\text{Li}$ Spectra at different temperatures as a function of field $H(T)$. In the inset the corrected echo integral intensity times the temperature as a function of temperature.

loss of signal most probably due to development of frozen magnetic regions in the sample below 20 K.

2. Spin-lattice relaxation rate, $1/T_1$

The spin-lattice relaxation rate ($1/T_1$) of ${}^7\text{Li}$ was measured by using a saturation recovery of the longitudinal magnetization using saturation pulse ($\frac{\pi}{2}|_{\text{sat}}$) of $10 \mu\text{s}$ at various temperatures from 93 K to 2.65 K. The saturation recovery curves are shown in the inset of Fig. 15. The curve above 7 K are best fitted with the single exponential function [$1 - \frac{M(t)}{M(0)} = A \exp(-\frac{t}{T_1})$] and below about 7 K are best fitted with a stretched exponential function [$1 - \frac{M(t)}{M(0)} = B \exp(-\frac{t}{T_1})^\beta + C$]. Here A & B denotes the saturation level of the signal and β is the stretching exponent. In general, the spin-glass systems possess a distribution of the spin-lattice relaxation times (T_1) due to the existence of different relaxation channels. That's why here, β determines the width of the distribution window. This stretched exponential characteristics of the saturation recovery data below about 7 K confirms the presence of discrete and local magnetic domains. The Fig. 15 shows the spin-lattice relaxation rate as a function of temperature. Below 20 K it starts to increase and at around 7 K it shows a peak. It appears that the onset of freezing of the magnetic regions starts around 20 K and at 7 K they lock into a spin-glass state. This supports the dc magnetic susceptibility as well as the magnetic heat capacity data which shows a hump just below 20 K.

3. Spin-spin relaxation rate, $1/T_2$

The inset of Fig. 16 shows the decay of the transverse nuclear magnetization data at 60 MHz with different temperatures. The data above 7 K are well fitted to a Gaussian modified exponential function [$\frac{M(t)}{M(0)} = M(0) \cdot \{\exp(-\frac{t}{T_{2G}})^2 \cdot \exp(-\frac{t}{T_2})\}$] and the data below 7 K are fitted with a stretched exponential function

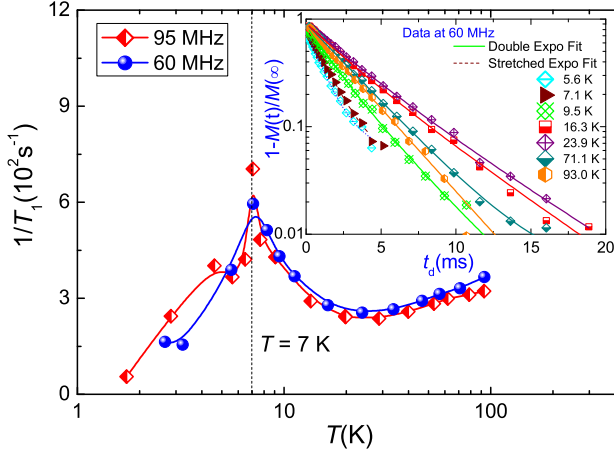


Figure 15: The spin-lattice relaxation rate as a function of temperatures at two frequencies 60 MHz and 95 MHz show ordering at 7 K. In the inset, the saturation recovery of the longitudinal magnetization as a function of the delay time at various temperatures. The solid and dashed lines are the best fit for single exponential function (above 7 K) and stretched exponential function (below 7 K) respectively.

[$\frac{M(t)}{M(0)} = A_2 \exp\left(\frac{-t}{T_2}\right)^\beta + C$]. From fitting, we obtained the T_2 values and plotted the spin-spin relaxation rate ($1/T_2$) as a function of temperature in Fig. 16. It shows that the spin-spin correlation begins to increase around 15 K with a peak at ≈ 3.2 K.

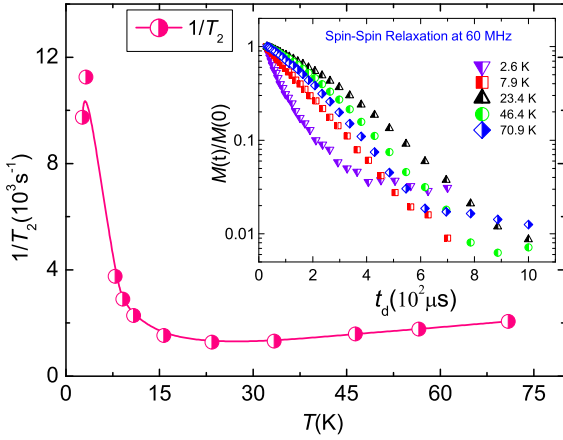


Figure 16: The temperature variation of the spin-spin relaxation rate $1/T_2$. The inset shows the decay of the transverse nuclear magnetization at some selected temperatures.

IV. CONCLUSIONS

With respect to the crystallography of polycrystalline LRMO we confirmed a single-phase nature from our XRD

investigation. In $\chi(T)$, ZFC-FC bifurcation was found below 4.45 K which is very much field sensitive. This ZFC-FC splitting suggests the presence of a glassy state. The frequency dependent χ_{ac} , where the freezing temperature (T_f) shifts towards higher T values as the frequency increases is a signature of glassy systems and thus it confirms the presence of the spin-glass ground state. Also, the out of phase component of the ac susceptibility $\chi_{ac}''(T)$ has a frequency dependence with an anomaly around T_f . The $\chi_{ac}''(T)$ is non-zero positive below T_f and is negative above T_f . This observation ruled out any bond disordered antiferromagnetic state. The characteristic frequency $\omega_0 \approx 1.01 \times 10^8$ rad/s obtained from the Vogel-Fulcher fit is less than that of conventional spin-glass systems (10^{13} rad/s), but the characteristic time $\tau_0 \approx 2.85 \times 10^{-10}$ s and critical exponent $zv \approx 4.88$ values are close to a conventional spin-glass [27]. This implies that the ground state of LRMO is more likely to be a conventional spin-glass. From heat capacity measurement, there occurs significant contribution of magnetic heat capacity and no sharp anomaly presents down to 2 K. The calculated magnetic entropy change $\Delta S_m = 8.55$ (J/mol K) is 75% of the theoretical value $R \ln(4)$ for this system. These numbers are not far from the usual LRO transition. However the change of entropy starts to decrease below 30 K, which is close to the CW temperature $|\theta_{CW}| = 26$ K also. From ^7Li NMR, there is no significant shift of the spectrum and the FWHM of spectra at high temperatures follows the Curie-Weiss behavior like dc susceptibility. The echo integral intensity times the T vs. T shows a drop below 20 K. This suggests a loss of signal probably due to development of frozen magnetic domains within the sample. In order to shed more light on the spin dynamics of Mn^{4+} ions, we have measured spin-lattice relaxation rate ($1/T_1$) and spin-spin relaxation rate ($1/T_2$) for ^7Li nuclei. Both show anomalies below 7 K like in the dc susceptibility indicating the spin-glass ground state of LRMO.

V. ACKNOWLEDGEMENT

SK acknowledges the discussion with Dr. Aga Shahee and R. K. Sharma and the financial support from IRCC, IIT Bombay. AVM would like to thank the Alexander von Humboldt foundation for financial support during his stay at Augsburg Germany. We kindly acknowledge support from the German Research Society (DFG) via TRR80 (Augsburg, Munich).

-
- [1] E. Dagotto, *Science* **309**, 257 (2005).
- [2] E. Dagotto and Y. Tokura, *MRS Bulletin* **33**, 1037 (2008).
- [3] Y. Tokura and N. Nagaosa, *Science* **288**, 462 (2000).
- [4] A. P. Ramirez, *Annual Review of Materials Science* **24**, 453 (1994).
- [5] J. E. Greedan, *J. Mater. Chem.* **11**, 37 (2001).
- [6] R. Moessner and A. P. Ramirez, *Physics Today* **59**, 24 (2006).
- [7] L. Balents, *Nature* **464**, 199 (2010).
- [8] J. G. Bednorz and K. A. Müller, *Zeitschrift für Physik B Condensed Matter* **64**, 189 (1986).
- [9] Y. Kamihara, T. Watanabe, M. Hirano, and H. Hosono, *J. Am. Chem. Soc.* **130**, 3296 (2008).
- [10] N. F. MOTT, *Rev. Mod. Phys.* **40**, 677 (1968).
- [11] Y. Tokura, *Colossal Magnetoresistive Oxides* (Gordon and Breach Science, New York, 2000).
- [12] A. Eftekhari, *Solid State Ionics* **161**, 41 (2003).
- [13] M. A. Arillo, G. Cuello, M. L. López, P. Martín, C. Pico, and M. L. Veiga, *Solid State Sciences* **7**, 25 (2005).
- [14] M. M. Thackeray, W. I. F. David, P. G. Bruce, and J. B. Goodenough, *Mater. Res. Bull.* **18**, 461 (1983).
- [15] Y. Okamoto, S. Niitaka, M. Uchida, T. Waki, M. Takigawa, Y. Nakatsu, A. Sekiyama, S. Suga, R. Arita, and H. Takagi, *Phys. Rev. Lett.* **101**, 086404 (2008).
- [16] R. Arita, K. Kuroki, K. Held, A. V. Lukoyanov, S. Skornyakov, and V. I. Anisimov, *Phys. Rev. B* **78**, 115121 (2008).
- [17] K. R. Knox, A. M. M. Abeykoon, H. Zheng, W.-G. Yin, A. M. Tsvelik, J. F. Mitchell, S. J. L. Billinge, and E. S. Bozin, *Phys. Rev. B* **88**, 174114 (2013).
- [18] G. Blasse, *J. Inorg. Nucl. Chem.* **25**, 743 (1963).
- [19] M. Onoda, H. Imai, Y. Amako, and H. Nagasawa, *Phys. Rev. B* **56**, 3760 (1997).
- [20] J. A. Mydosh, *Spin Glasses: An Experimental Introduction* (Taylor & Francis, London, 1993).
- [21] H. M. Rietveld, *J. Appl. Cryst.* **2**, 65 (1969).
- [22] J. Rodriguez-Carvajal, *Physica B: Condensed Matter* **192**, 55 (1993).
- [23] K. Momma and F. Izumi, *J. Appl. Cryst.* **44**, 1272 (2011).
- [24] K. Binder and A. P. Young, *Rev. Mod. Phys.* **58**, 801 (1986).
- [25] C. A. M. Mulder, A. J. van Duynveldt, and J. A. Mydosh, *Phys. Rev. B* **23**, 1384 (1981).
- [26] R. Mahendiran, Y. Bréard, M. Hervieu, B. Raveau, and P. Schiffer, *Phys. Rev. B* **68**, 104402 (2003).
- [27] Q. Luo, D. Q. Zhao, M. X. Pan, and W. H. Wang, *Appl. Phys. Lett.* **92**, 011923 (2008).
- [28] D. S. Fisher and D. A. Huse, *Phys. Rev. Lett.* **56**, 1601 (1986).
- [29] J. Dho, W. S. Kim, and N. H. Hur, *Phys. Rev. Lett.* **89**, 027202 (2002).
- [30] Y. Sun, M. B. Salamon, K. Garnier, and R. S. Averback, *Phys. Rev. Lett.* **91**, 167206 (2003).
- [31] T. Chakrabarty, A. V. Mahajan, and S. Kundu, *Journal of Physics: Condensed Matter* **26**, 405601 (2014).
- [32] A. Bhattacharyya, S. Giri, and S. Majumdar, *Phys. Rev. B* **83**, 134427 (2011).
- [33] B. Maji, K. G. Suresh, and A. K. Nigam, *Journal of Physics: Condensed Matter* **23**, 506002 (2011).
- [34] M. Sasaki, P. E. Jönsson, H. Takayama, and H. Mamiya, *Phys. Rev. B* **71**, 104405 (2005).